BULLETIN OF THE POLISH ACADEMY OF SCIENCES
TECHNICAL SCIENCES, Vol. 62, No. 1, 2014
DOI: 10.2478/bpasts-2014-0019

Vertical vibrations of composite bridge/track structure/high-speed train systems. Part 2: Physical and mathematical modelling

M. PODWORNA[1] and M. KLASZTORNY[2*]

[1] Institute of Civil Engineering, Wroclaw University of Technology, 27 Wyspianskiego St., 50-370 Wroclaw, Poland
[2] Department of Mechanics and Applied Computer Science, Military University of Technology, 2 Kaliskiego St., 00-908 Warsaw, Poland

Abstract. A theory of one-dimensional physical and mathematical modelling of the composite (steel-concrete) bridge/track structure/high-speed train system is developed including viscoelastic suspensions of rail-vehicles with two two-axle bogies each, non-linear Hertz contact stiffness and one-sided contact between wheel sets and rails, the viscoelastic and inertia features of the bridge, the viscoelastic track structure on and beyond the bridge, approach slabs, and random vertical track irregularities. Compared to the state-of-the-art, the physical model developed in the study accurately reproduces dynamic processes in the considered system. Division of the system into the natural subsystems, a method of formulation of the equations of motion partly in implicit form and the finite element method are applied. Vibrations in the vertical plane of symmetry are described by more than nine matrix equations of motion with constant coefficients. Couplings and non-linearity are hidden in the generalized load vectors. The equations of motion are integrated using the implicit Newmark average acceleration method with linear extrapolation of the interactions between the subsystems.

Key words: composite steel-concrete bridge, ballasted track structure, high-speed train, random track irregularities, FE modelling, equations of motion.

1. Introduction

Composite (steel-concrete) bridges loaded by high-speed trains need to be designed or modernized to ensure the traffic safety condition (TSC) and the passenger comfort condition (PCC). Too large vertical accelerations of the bridge platform may cause ballast destabilization in the track structure. Railway track irregularities are considered to be one of the main factors affecting dynamic response of a composite bridge/track structure/high speed train system (BTT). So far, theoretical studies on the effect of track irregularities on vibrations of a railway bridge loaded by a high-speed train have been conducted on one-dimensional/three-dimensional (1D/3D) simplified models of the BTT system. Railway track irregularities are due to track formation technology, subsidence, contemporary mechanical maintenance, soil settlement and other factors. Experimental measurements and/or modelling of track irregularities are considered in a number of papers, e.g. [1–3]. The common model of railway track irregularity vertical profiles is a stationary and an ergodic Gaussian process in space. A track irregularity vertical profile is characterised by a one-sided power spectral density (PSD) function. The PSD function corresponding to line grades 1 to 6 from American Railway Standard was elaborated by USA Federal Railroad Administration (FRA).

Dynamic responses of bridges due to high-speed trains are usually described by means of dynamic amplification factors, bridge deck accelerations and car body accelerations [4]. The UIC (Draft) Code 776-2, "Design requirements for rail bridges based on interaction phenomena between train, track, bridge and in particular speed", Paris, France, Union Int. des Chemins de Fer (2003) specifies the following conditions: the TSC expressed by the ultimate vertical acceleration of the bridge deck, i.e. $a_{\mathrm{p,lim}} = 0.35\mathrm{g} = 3.43$ m/s^2, the PCC expressed by the ultimate vertical deflection of the bridge span, i.e. $w_{\mathrm{lim}} = L/1700$, where L is the bridge span length. The maximum permitted peak values of bridge deck acceleration 3.50 m/s^2 for ballasted track is recommended in EN 1991-2 Eurocode 1: "Actions on structures, Part 2: General actions – traffic loads on bridges" and EN 1990 Eurocode: "Basis of structural design, Annex A2: Application for bridges. Check on bridge deformations, performed for PCC", can be related to the vertical deflection of the deck or directly to the coach body vertical acceleration. The indicative levels of comfort, expressed by the vertical acceleration inside the coach during the travel, are specified in EN 1990 Eurocode: "Basis of structural design, Annex A2: Application for bridges" are cited in [5].

The review of state-of-the-art till 1986 in dynamics of railway bridges under high-speed trains is presented in [6]. The update of this review till the year 2004 is included in [7]. This paper presents the state-of-the-art, in a concise form, related to the past 10 years, in the field of modelling and numerical studies of railway bridges under high-speed trains.

Fryba [8] presents a prediction of the forced resonances in single-span single-track railway bridges. The bridge is modelled viscoelastically as an Euler beam, while the train is mapped by a stream of moving forces of the cyclic structure. The writer analysed the series-of-types of concrete and steel bridges using the Galerkin method. Cheng et al. [9] examined the planar linear model of the bridge/track/moving

*e-mail: m.klasztorny@gmail.com

train system incorporating a finite element in the form of two Euler beams connected with the viscoelastic layer, loaded by moving double-mass oscillators.

Au et al. [10] analyze a railway cable-stayed bridge with a total length of 750 m, subjected to a moving train. They adopted a planar model and the FEM discretization of the bar bridge superstructure. The basic model of a moving vehicle supported on two two-axle bogies is the Matsuura model with 6 degrees of freedom (6DOF). The method of explicit formulating the equations of motion in matrix notation is applied. Zhang *et al.* [11] model the 3D BTT system using bar finite elements to discretise the bridge superstructure and rails. The track superstructure is reflected by the Winkler foundation. A rail-vehicle is a multibody system with viscoelastic suspensions, both horizontal and vertical, of the first and second stage. Wheels are treated as sprung masses, according to the Hertz theory.

Au et al. [3] have developed a 1D vibration study on railway cable-stayed bridges under moving trains, taking into account random rail irregularities. The main girder of the bridge is modelled using 6DOF Euler beam finite elements and taking into account the linear and geometric stiffness matrices. Double-side constraints between the moving wheel set unsprung masses and the rails are assumed. The track structure is neglected. The matrix equation of motion of the bridge/moving train system is formulated in the explicit form. Sample vertical profiles of random rail roughness, considered as stationary and ergodic processes in space, are generated using the empirical formula for PSD function with the parameters corresponding to the USA quality classes 1–6.

Song and Hoi [12] present numerical studies of the double-track bridge/moving TGV train. The writers considered continuous beam bridges using 6DOF beam finite elements for the discretization, including two boundary torsional angles, and took into account the Jacobs bogies. The explicit form of the matrix equation of motion was applied.

Podworna [13, 14] develops a 1D theory of modelling BTT systems. The bridge superstructure is modelled as a stepwise prismatic viscoelastic Timoshenko beam. The rails are mapped by a continuous viscoelastic prismatic Euler beam. Fasteners and ballast-bed are physically nonlinear and sleepers are point masses vibrating vertically. The track bed (subsoil) is reflected by a set of equidistant single mass viscoelastic oscillators. The train is composed of vehicles each modelled by a 6DOF Matsuura system.

Lu et al. [15] adopted the vehicle – bridge interaction (VBI) element in non-stationary random vibration analysis of vehicle/bridge systems. The VBI element condenses DOFs of the vehicle into those of the bridge by using the Newmark integration scheme. The bridge is reflected by a prismatic beam discretised with Euler beam finite elements. The train is composed of a number of vehicles, each reflected by the 6DOF Matsuura four-axle model.

Dynamic response of an existing bridge subjected to different moving trains is developed in [4], including track irregularities and neglecting snaking of wheel sets. The research was carried out using the 3D dynamic bridge – train interaction (DBTI) model, in which the inertia forces of the moving unsprung train axles are coupled with the bridge.

The study develops an advanced theory of 1D physical and mathematical modelling of composite (steel-concrete) bridge/track structure/high-speed train systems, taking into consideration viscoelastic suspensions of four-axle rail-vehicles, non-linear Hertz contact stiffness and one-sided contact between the wheel sets and the rails, the viscoelastic and inertia features of the bridge, the viscoelastic track structure on and beyond the bridge, approach slabs, and random vertical track irregularities. Compared to the state-of-the-art, the physical model developed in the study accurately reproduces dynamic processes in BTT systems. The system is divided into the natural subsystems. Continuous viscoelastic subsystems are modelled numerically using the finite element method (FEM). Matrix equations of motion of the subsystems are formulated partly in implicit form.

2. Physical and mathematical modelling of BTT systems

2.1. Assumptions. The bridge/track structure/high-speed train system (BTT) is composed of a simply supported composite (steel-concrete) bridge, two approach slabs, a track structure with continuously welded rails and adapted to high operating speeds and a high-speed train. The following assumptions are adopted in physical and numerical modelling of this system:

- There is considered a finitely long deformable welded track including the out-of-transition zones, the transition zones and the bridge zone. The track outside of these zones is non-deformable and straight.
- The axis of the track is a horizontal straight line. There are random vertical track irregularities resulting from construction and maintenance of the track, as well as settlement of ballast and subgrade. Random vertical track irregularities are identical for both main rails.
- Vertical track irregularities are described by a spatial function $r(x)$ which is a stationary ergodic Gaussian process defined by the PSD function determined experimentally.
- The BTT system has a vertical plane of symmetry coinciding with the track axis; this is the plane of vibration. There are only vibrations in this plane, commonly termed as vertical vibrations. The modelling is therefore 1D.
- The operating and side rails are viscoelastic prismatic beams deformable in flexure.
- The rail-sleeper fasteners are viscoelastic elements with the non-linear elastic characteristic.
- The sleepers vibrate vertically and are modelled as concentrated masses.
- Macadam ballast is modelled as a set of vertical viscoelastic constraints with the non-linear elastic characteristic. The model includes the possibility of detachment of the sleepers from the ballast. The lumped ballast model is used. Each sleeper is supported viscoelastically.
- Track bed (subsoil) is a linearly viscoelastic layer modelled discretely.

- Approach slabs are modelled as viscoelastic prismatic beams deformable in flexure. Each slab is supported on one edge on the abutment. The slab material is viscoelastic.
- The bridge superstructure is reflected by a simply-supported step-wise prismatic beam, deformable in flexure, symmetrical relative to the bridge midspan. The superstructure materials (steel, concrete) are viscoelastic.
- A cross-section of the bridge superstructure and the platform is symmetrical about the vertical axis. Vibration coupling of twin spans over the ballast does not occur. Connection of the reinforced concrete slab with the main steel beams is non-deformable.
- Rail-vehicles form a high-speed ICE-3 German train. Each vehicle has two independent two-axle bogies. The planar Matsuura model of a rail-vehicle is adopted in the extended version formed by incorporating non-linear one-sided contact Hertz springs at wheel set – rail contacts. Potential micro separations and impacts of moving wheels in reference to the main rails are taken into account.
- The train operating velocity is constant and belongs to the interval 30–300 km/h.
- Vibrations of the BTT system are physically nonlinear and geometrically linear.

2.2. Concept of physical and numerical modelling. A finitely long section of the deformable track is depicted in Fig. 1. The out-of-approach zones have length of 2D. The first D section from the train entering side enters subsequent vehicles into the quasi-stationary random vibration state. The VVRZ zone (Vehicle Vibration Registration Zone) is the area of registration of the design quantities found in the traffic safety condition (TSC) and in the passenger comfort condition (PCC). The BVRZ zone (Bridge Vibration Registration Zone) is the area of registration of vibrations and stresses in reference to the bridge superstructure and the platform. The wheel set/rails interaction forces are recorded during the passage of the selected axle over the VVRZ zone, including micro separations of the wheels from the rails and impacts.

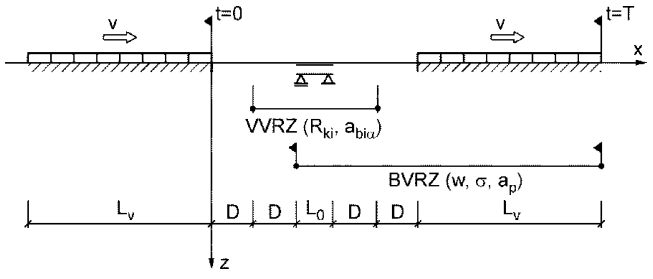

Fig. 1. Schematic diagram of BTT system at time $t = 0$ and $t = T$

The dynamic process is simulated within the range of $t \in [0, T]$, where $T = (4D + L_o + L_v)/v$, with: L_o – bridge span length plus length of approach slabs plus two sleeper intervals, L_v – train set length, v – operating velocity (horizontal velocity of moving load).

The remaining symbols in Fig. 1 denote: $w(x,t)$ – vertical deflection of bridge superstructure, $\sigma(x,t)$ – longitudinal normal stresses in bottom fibres of main beams, t – time variable, x, y – coordinates, $a_p(x,t)$ – vertical acceleration of bridge platform, $R_{ki}(t)$, $k = 1,2,3,4$, $i = 1,2,\ldots,N_v$ – dynamic pressures of moving wheel sets, $k = 1,2,3,4$ – numbering of wheel sets of i^{th} vehicle, N_v – number of vehicles forming train, $a_{bi\alpha}(t)$, $i = 1,2,\ldots,N_v$, $\alpha = f, r$ – vertical accelerations of suspension pivots in car-bodies (f, r – front/rear bogie, respectively), T – dynamic process duration time.

Non-stationary vibrations of the bridge caused by the passage of a high-speed train across the bridge is recorded in the interval $vt \in [2D; 4D + L_o + L_v]$ [m]. The outside sections D eliminate distortion in the response of vehicles caused by finitely long sections of the deformable track in the out-of-approach zones. Transient vibrations of subsequent rail-vehicles are recorded in intervals of $u_i = vt - (i-1)\,l \in [D; 3D + L_o]$ [m], $i = 1,2,\ldots,N_v$, where l denotes rail-vehicle length.

Random vertical track irregularities occur in the $4D + L_o$ zone (Fig. 2). In order to eliminate unrealistic impacts at the ends of this zone, respective constant shifts in the displacement are made outside the deformable track zone, equal to $r(0)$ and $r(4D + L_o)$, respectively.

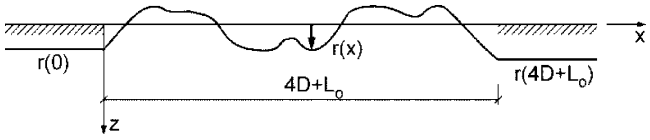

Fig. 2. Random vertical track irregularities in $4D + L_o$ zone

A 1D physical model of the track structure/bridge subsystem is presented in Fig. 3. A constant sleeper spacing d is used to discretize the subsystem. The main rails are fixed at the ends of the finite-long section of track, $4D + L_o$. The side rails have length of L_o and are rested viscoelastically on the sleepers. Viscoelastic elements modelling the fasteners and the ballast incorporate physically nonlinear elastic constraints. Discretization of beams modelling operating rails, side rails, approach slabs and the bridge superstructure uses finite elements deformed in flexure, with 4DOF and length d. The nodes of the finite elements coincide with the positions of sleepers. Detailed description of physical and numerical modelling of the track structure/bridge subsystem as well as symbols of the structural parameters used in Fig. 3 are presented in the next section.

The ballast mass on the approach slabs and the bridge is included in the distributed form. Step-wise changes in the parameters of the bridge superstructure occur in respective nodes of the finite element mesh (Figs. 3, 4). The physical model of the track / bridge subsystem is symmetrical relative to the midspan, with the exception of track irregularities which are random. The symbols used in Fig. 4 are denoted in the next section.

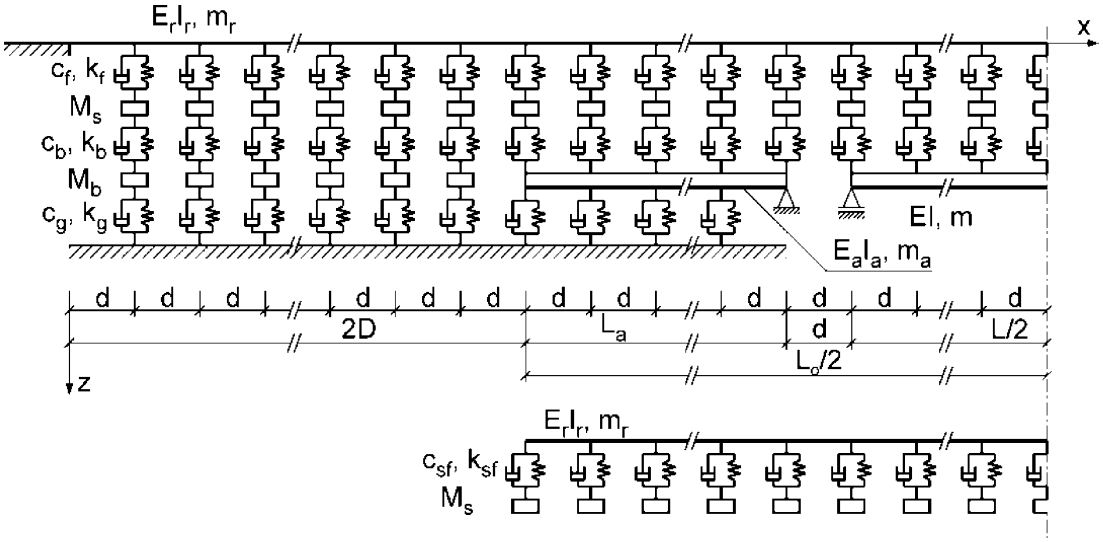

Fig. 3. 1D physical model of track structure/bridge subsystem

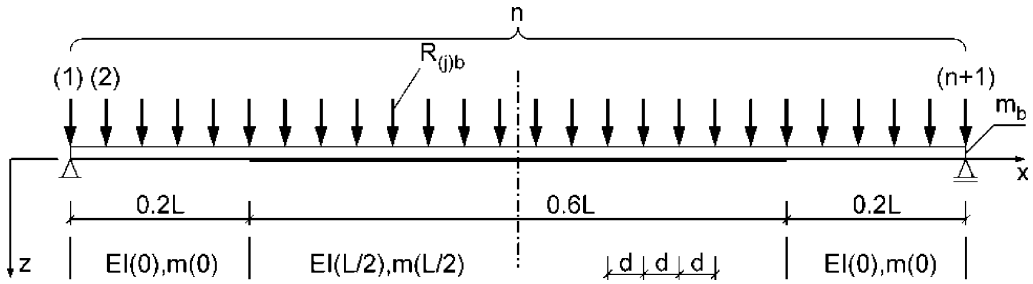

Fig. 4. 1D physical model of bridge loaded with subset of interaction forces carried by ballast

The BTT system has the following natural inertial subsystems (Figs. 1, 3): BS – bridge superstructure, LAS – left approach slab, RAS – right approach slab, LB – left ballast-bed, RB – right ballast-bed, SL – sleepers, OR – operating rails, SR –side rails, RVi, $i = 1, 2, \ldots, N_v$ – rail-vehicles. These subsystems are subject to the relevant subsets of vertical interaction forces, carried by elastic/viscoelastic physically linear/nonlinear constraints. Using Lagrange's equations and the internal assembling, one obtains linear matrix equations of motion of individual subsystems with the generalized load vectors stored in an implicit form. Linear/non-linear interaction forces are transformed into the generalized load vectors. This formulation leads to equations of motion of the subsystems with constant coefficients. Coupling and non-linearity of the subsystems is hidden in the generalized load vectors expressed by the interaction forces.

The method of physical and numerical modelling of the BTT system enables formulation of matrix equations of motion of the system in relatively easy way, and reduces the CPU time by several times compared with the models in the explicit form [7]. Transient vibrations of the BTT system are described by $8 + N_v$ matrix equations of motion.

2.3. Determination of matrix equations of motion of subsystems Bridge superstructure (BS). A model of the bridge superstructure constitutes a simply supported beam with symmetrical segmental prismatic mass and flexural stiffness distribution, as shown in Fig. 4. Damping of the superstructure is described by the Rayleigh viscous damping model. The BS subsystem is described by parameters L, d and m – mass per unit length (including additional mass), $m(0)$ – mass m for $\overline{x} \in [0; 0.2L)\,(0.8L; L]$, $\overline{x} = x - (2D + L_a + d)$, $m(L/2)$ – mass m for $\overline{x} \in [0.2L; 0.8L]$, $\overline{x} = x - (2D + L_a + d)$, EI – flexural stiffness, $EI(0)$ – flexural stiffness, EI for $\overline{x} \in [0; 0.2L)\,(0.8L; L]$, $EI(L/2)$ – flexural stiffness, EI for $\overline{x} \in [0.2L; 0.8L]$, γ – fraction of quasi-constant damping in frequency range $[f_1 f_2]$, μ, κ – Rayleigh's damping coefficients, m_b – ballast mass per unit length, n– number of finite elements of d length, $W_b = W_b(L/2)$ – bending index for bottom fibres in reference to cross-section at midspan.

The symbol L_a denotes the theoretical length of an approach slab. Additional mass added to the bridge superstructure mass consists of levelling concrete, isolation, curbs, service footway, external cables and the others.

The finite element nodes correspond to positions of sleepers used in steps d. The classical bent Euler beam finite element is applied with 4DOF (Fig. 5). Deflection of an element is approximated with Hermite polynomials of the third degree, i.e.:

$$w_e\,(\overline{x}, t) = \mathbf{q}_e^T\,(t)\,\mathbf{s}(\overline{x}), \tag{1}$$

where

$$\mathbf{q}_e\,(t) = \mathrm{col}(q_{1'}\ q_{2'}\ q_{3'}\ q_{4'}),$$
$$\mathbf{s}\,(\overline{x}) = \mathbf{H}\mathbf{h}\,(\xi)\,, \qquad \xi = \frac{\overline{x}}{d},$$
$$\mathbf{H} = \begin{bmatrix} 1 & 0 & -3 & 2 \\ 0 & d & -2d & d \\ 0 & 0 & 3 & -2 \\ 0 & 0 & -d & d \end{bmatrix}, \qquad \mathbf{h}(\xi) = \begin{bmatrix} 1 \\ \xi \\ \xi^2 \\ \xi^3 \end{bmatrix}. \tag{2}$$

The elastic energy and the kinetic energy of the finite element e are described by well-known integral formulae that give the following matrix results

$$E_{se} = \frac{1}{2}EI_e \int_0^d \left(\frac{\partial^2 w_e}{\partial \overline{x}^2}\right)^2 d\overline{x} = \frac{1}{2}\mathbf{q}_e^T \mathbf{K}_e \mathbf{q}_e,$$
$$E_{ke} = \frac{1}{2}m_e \int_0^d \left(\frac{\partial w_e}{\partial t}\right)^2 d\overline{x} = \frac{1}{2}\dot{q}_e^T \mathbf{B}_e \dot{q}_e, \tag{3}$$

where $(\dot{}) = d/dt$ and

$$\mathbf{K}_e = \frac{EI_e}{d^3}\mathbf{H}\mathbf{D}^2\mathbf{U}\left(\mathbf{H}\mathbf{D}^2\right)^T, \qquad \mathbf{B}_e = m_e d\mathbf{H}\mathbf{U}\mathbf{H}^T \tag{4}$$

while

$$\mathbf{D} = \begin{bmatrix} 0 & 0 & 0 & 0 \\ 1 & 0 & 0 & 0 \\ 0 & 2 & 0 & 0 \\ 0 & 0 & 3 & 0 \end{bmatrix},$$

$$\mathbf{U} = \int_0^1 \mathbf{h}\mathbf{h}^T d\xi = \begin{bmatrix} 1 & \frac{1}{2} & \frac{1}{3} & \frac{1}{4} \\ & \frac{1}{3} & \frac{1}{4} & \frac{1}{5} \\ & & \frac{1}{5} & \frac{1}{6} \\ \text{symm.} & & & \frac{1}{7} \end{bmatrix} \tag{5}$$

and

$$EI_e = EI, \qquad m_e = m + m_b. \tag{6}$$

Values of parameters EI, m depend on the global coordinate x corresponding to the position of the finite element.

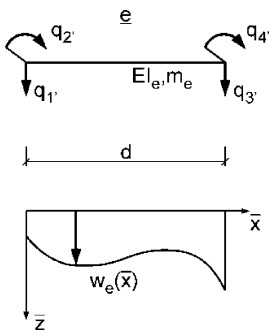

Fig. 5. Classical bent Euler beam finite element with 4DOF

Figures 6, 7 show sets of generalized coordinates in the track/bridge subsystem. The beam reflecting the superstructure is described by vector $\mathbf{q} = \mathrm{col}(q_1\ q_2\ \ldots\ q_N)$ with $N = 2n$.

As a result of aggregation of the finite elements, one obtains the following quadratic forms that define the elastic energy and the kinetic energy of the BS subsystem:

$$E_s = \frac{1}{2}\mathbf{q}^T\mathbf{K}\mathbf{q}, \qquad E_k = \frac{1}{2}\dot{\mathbf{q}}^{\mathrm{T}}\mathbf{B}\dot{\mathbf{q}}. \tag{7}$$

The stiffness matrix $\mathbf{K}$ and the inertia matrix $\mathbf{B}$ have band symmetrical structure with the band width of 4. The beam is a straight line graph, with the 0-1 transformation of the generalized coordinates to the local coordinates, so the aggregation takes place by the formulae:

$$[\mathbf{K}]_{ij} := [\mathbf{K}]_{ij} + [\mathbf{K_e}]_{i'j'}\,, \qquad [\mathbf{B}]_{ij} := [\mathbf{B}]_{ij} + [\mathbf{B_e}]_{i'j'} \tag{8}$$

while $i = i\,(i')$, $j = j\,(j')$ are described by respective incidence matrix $\mathbf{q}/\mathbf{q}_e$, := is a completion operation, $e = 1, 2, \ldots, n$, $i'j' = 1', 2', 3', 4'$.

The damping power of the beam and the damping matrix in accordance with the Rayleigh model have the form [16]

$$\Phi = \frac{1}{2}\dot{\mathbf{q}}^T\mathbf{C}\dot{\mathbf{q}}, \qquad \mathbf{C} = \mu\mathbf{B} + \kappa\mathbf{K}. \tag{9}$$

The parameters $\mu\kappa$ are determined from the system of the following linear algebraic equations

$$\begin{cases} \dfrac{\mu}{\omega_l} + \varkappa\omega_l = 2\gamma, \\ \dfrac{\mu}{\omega_u} + \varkappa\omega_u = 2\gamma, \end{cases} \tag{10}$$

where $\omega_l\omega_u$ – circular frequencies that correspond to the exact value of damping ratio γ with the critical value $\gamma_{cr} = 1$ (Fig. 8, [16]). Frequencies $f_l = \dfrac{\omega_l}{2\pi}$, $f_u = \dfrac{\omega_u}{2\pi}$ are adopted so that the interval $[f_l,\ f_u]$ covers the beam modal systems that affect the dynamic response, e.g. $f_l = 1$ Hz, $f_l = 1000$ Hz. In the interval $[f_l,\ f_u]$ damping of the system is quasi-constant. Note that in Ref. [16] parameter γ has different meaning.

The solution of the equation system (10) has the form

$$\mu = 2\gamma\frac{\omega_l\omega_u}{\omega_l + \omega_u} = 4\pi\gamma\frac{f_l f_u}{f_l + f_u},$$
$$\kappa = 2\gamma\frac{1}{\omega_l + \omega_u} = \frac{\gamma}{\pi}\frac{1}{f_l + f_u}. \tag{11}$$

Load of the beam constitute the interaction forces which are carried by the ballast-bed. They are respective subset of elements of the vector $\mathbf{R}_b = \mathrm{col}\,(R_{1b}\,R_{2b}\ldots R_{n_t b})$ where $n_t = 2n_a + 2n_b + n + 5$ n_a – number of finite elements corresponding to approach slab, $(n_b + 2)$ –number of finite elements corresponding to operating rails in left or right out-of-approach zone (Figs. 9, 10). The beam is loaded by the nodal forces $R_{(j)b}$, $(j) = (1)\,(2), \ldots, (n+1)$ with $(j) = j + n_a + n_b + 2$, $j = 1, 2, \ldots, n+1$.

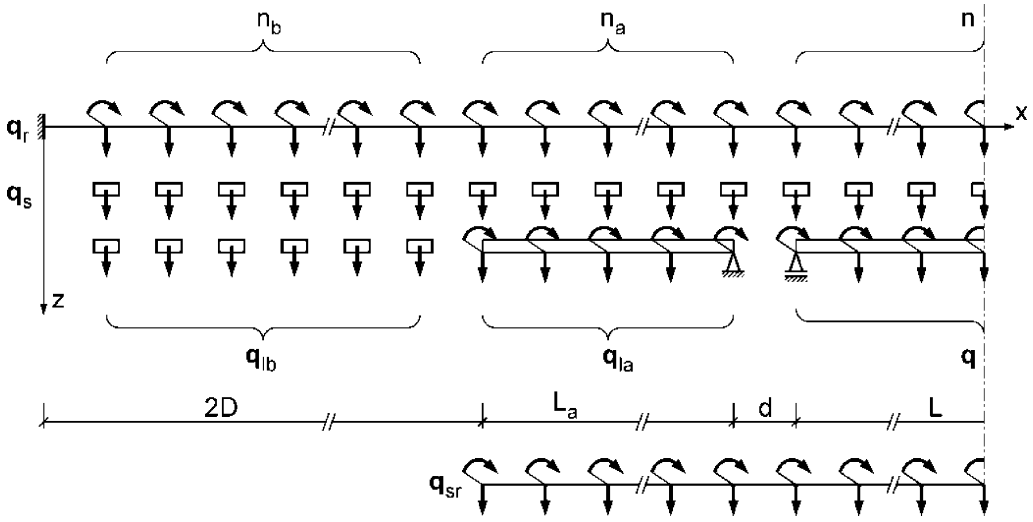

Fig. 6. Subsets of generalized coordinates of track / bridge subsystem to left of centre line

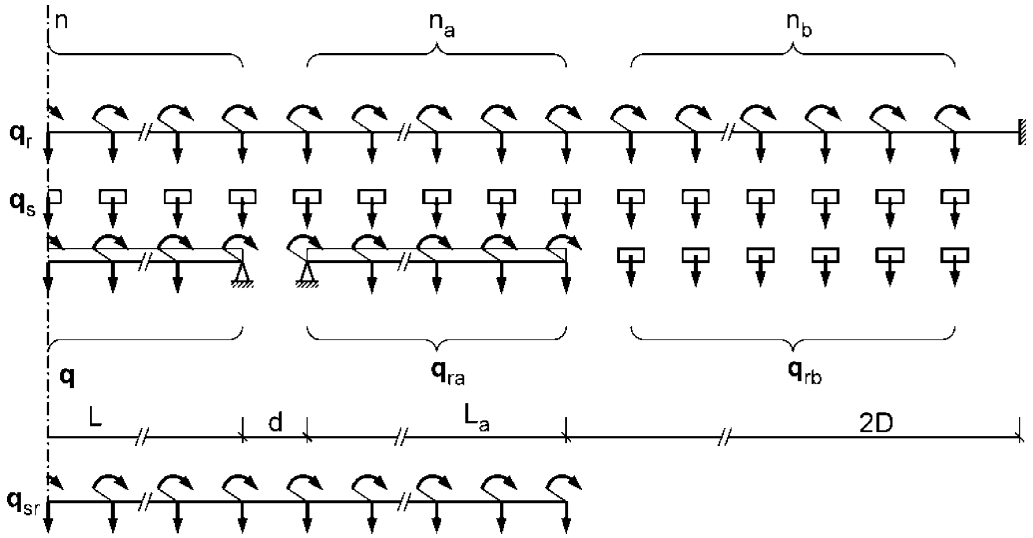

Fig. 7. Subsets of generalized coordinates of track / bridge subsystem to right of centre line

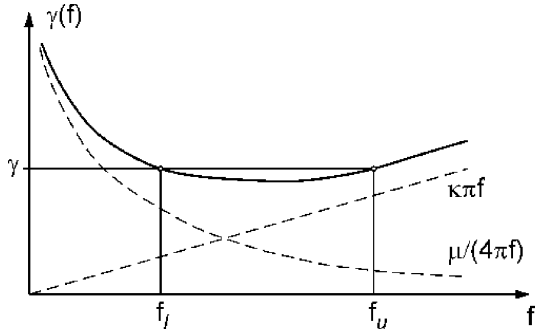

Fig. 8. Interpretation of parameters μ, κ in Rayleigh damping model of discrete systems ([16], page 27)

Virtual work of nodal forces $R_{(j)b}$ on vertical displacements of the beam is

$$L = \mathbf{q}^T \mathbf{F}, \tag{12}$$

where $\mathbf{F}$ is a vector of generalized loads calculated according to the formula

$$\mathbf{F} = \mathrm{col}(0\ R_{(2)b}\ 0\ R_{(3)b}\ 0 \ldots R_{(n)b}\ 0). \tag{13}$$

After inserting the forms (7), $(9)_1$, (12) to the Lagrange equations of the second kind, i.e.

$$\frac{d}{dt}\mathrm{grad}\, E_k\left(\dot{\mathbf{q}}\right) + \mathrm{grad}\, \Phi\left(\dot{\mathbf{q}}\right) + \mathrm{grad}\, E_s\left(\mathbf{q}\right) = \mathrm{grad}\, L(\mathbf{q}) \tag{14}$$

one obtains a matrix equation of motion of the BS subsystem partly in implicit form, i.e.

$$\mathbf{B}\ddot{\mathbf{q}} + \mathbf{C}\dot{\mathbf{q}} + \mathbf{K}\mathbf{q} = \mathbf{F}. \tag{15}$$

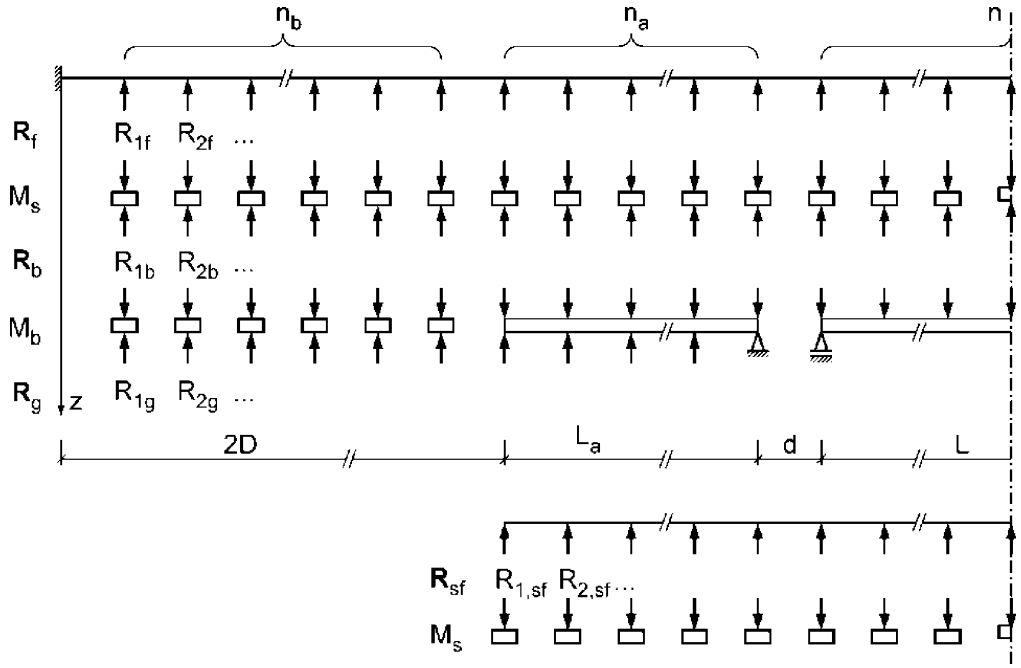

Fig. 9. Subsets of interaction forces in track / bridge subsystem to left of centre line

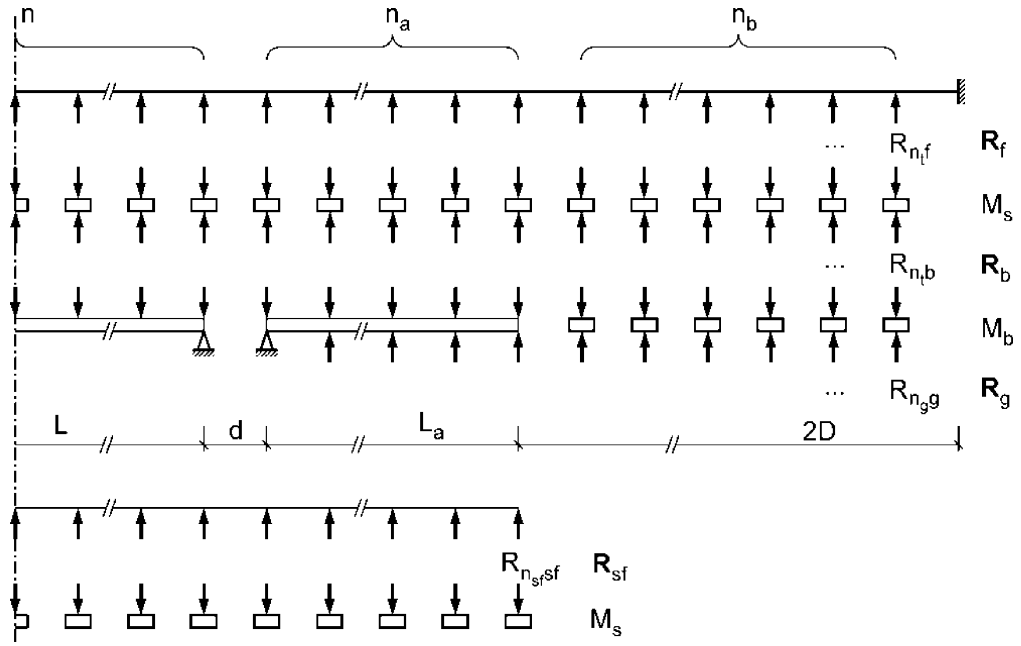

Fig. 10. Subsets of interaction forces in track / bridge subsystem to right of centre line

Time-histories of bending moments and longitudinal normal stresses in the bottom fibres of the finite element e, in which the midspan is included, are determined by formulae

$$M_e(\overline{x},t) = -EI_e\frac{\partial^2 w_e}{\partial \overline{x}^2} = -\frac{EI_e}{d^2}\mathbf{q}_e^T(t)\,\mathbf{H}\mathbf{D}^2\mathbf{h}(\xi),$$
$$\sigma_e(\overline{x},t) = \frac{M_e(\overline{x},t)}{W_b}, \tag{16}$$

where:

a) for n even: $e = 0.5n$,$\overline{x} = d$,

b) for n odd: $e = [0.5n] + 1$, $\overline{x} = 0.5d$.

Left approach slab (LAS). The left approach slab is modelled as a viscoelastic prismatic beam deformable in flexure and supported at the right end, Fig. 3. Damping is described by the Rayleigh model. The LAS subsystem is described by parameters L_a, d, m_b and m_a – mass per unit length, E_aI_a – flexural stiffness, γ_a – quasi-constant damping ratio in frequency range $[f_l f_u]$, μ_a, κ_a – damping coefficients of the Rayleigh model, n_a – number of finite elements of d length.

The finite element nodes correspond to positions of sleepers used in steps d. The bent Euler beam finite element with 4DOF is used, as shown in Fig. 5. The deflection, kinetic and

elastic energy of an element are described by Eqs. (1)–(5), wherein

$$EI_e = E_a I_a, \qquad m_e = m_a + m_b. \tag{17}$$

Figure 6 shows a set of coordinates related to the LAS beam, forming vector $\mathbf{q}_{la}= \mathrm{col}\,(q_{1,la}\ q_{2,la}\ \ldots\ q_{N,la})$ wherein $N= 2n_a+1$.

As a result of aggregation of the finite elements one obtains the elastic energy and the kinetic energy of the LAS subsystem as

$$E_{s,la} = \frac{1}{2}\mathbf{q}_{la}^T\mathbf{K}_{la}\mathbf{q}_{la}, \qquad E_{k,la} = \frac{1}{2}\dot{\mathbf{q}}_{la}^T\mathbf{B}_{la}\dot{\mathbf{q}}_{la}, \tag{18}$$

where

$$\begin{aligned}[\mathbf{K_{la}}]_{ij} &:= [\mathbf{K}_{la}]_{ij} + [\mathbf{K}_e]_{i'j'}\,,\\ [\mathbf{B}_{la}]_{ij} &:= [\mathbf{B}_{la}]_{ij} + [\mathbf{B}_e]_{i'j'}\,,\end{aligned} \tag{19}$$

wherein $i = i\,(i')\,, j = j(j')$ are defined by respective incidence matrix $\mathbf{q}_{la}/\mathbf{q}_e$; $e= 1, 2, \ldots, n_a$; $i', j' = 1', 2', 3', 4'$.

The damping power of the LAS beam and the damping matrix in accordance with the Rayleigh model have the form

$$\Phi_{la} = \frac{1}{2}\dot{\mathbf{q}}_{la}^T\mathbf{C}_{la}\dot{\mathbf{q}}_{la}, \qquad \mathbf{C}_{la}= \mu_a\mathbf{B}_{la} + \kappa_a\mathbf{K}_{la}, \tag{20}$$

where (*vide* Eq. (11))

$$\mu_a= 4\pi\gamma_a\frac{f_l f_u}{f_l + f_u}, \qquad \kappa_a = \frac{\gamma_a}{\pi}\frac{1}{f_l + f_u}. \tag{21}$$

Load of the LAS beam constitute appropriate subsets of interaction forces transmitted through the ballast and interaction forces transmitted through the subsoil (Figs. 3, 9). The forces charging the LAS beam are specified below:

$$\begin{gathered}R_{(j)b}\,;\ (j) = (1)\,(2)\,, \ldots, (n_a{+}1)\,;\\ (j) = j + n_b{+}1;\ j{=}\ 1, 2, \ldots, n_a{+}1,\\ R_{(j)g}\,;\ (j) = (1)\,(2)\,, \ldots, (n_a)\,;\\ (j) = j + n_b{+}1;\ j{=}\ 1, 2, \ldots, n_a.\end{gathered}$$

The virtual work of these forces on vertical displacements of the LAS beam is

$$L_{la} = \mathbf{q}_{la}^T\mathbf{F}_{la}, \tag{22}$$

where

$$\begin{aligned}\mathbf{F}_{la}{=}\ \mathrm{col}(&R_{(1)b}{-}R_{(1)g}\ 0\ R_{(2)b}{-}R_{(2)g}\ 0\ \ldots\\ &R_{(n_a)b}{-}R_{(n_a)g}\ 0\ 0).\end{aligned} \tag{23}$$

After inserting forms (18), $(20)_1$, (22) for the Lagrange equations of the second kind, i.e.

$$\begin{aligned}\frac{d}{dt}\mathrm{grad}\,E_{k,la}\,(\dot{\mathbf{q}}_{la}) + \mathrm{grad}\,\Phi_{la}\,(\dot{\mathbf{q}}_{la}) + \mathrm{grad}\,E_{s,la}\,(\mathbf{q}_{la})\\ = \mathrm{grad}\,L_{la}(\mathbf{q}_{la})\end{aligned} \tag{24}$$

one obtains a matrix equation of motion of the LAS subsystem partly in implicit form, i.e.

$$\mathbf{B}_{la}\ddot{\mathbf{q}}_{la} + \mathbf{C}_{la}\dot{\mathbf{q}}_{la} + \mathbf{K}_{la}\mathbf{q}_{la} = \mathbf{F}_{la}. \tag{25}$$

Right approach slab (RAS). Physical and numerical modelling of the right approach slab is analogous to the left one. The right approach slab is modelled as a viscoelastic prismatic beam deformable in flexure, simply supported at the left end, Fig. 7. The RAS subsystem is described by the same parameters as the LAS subsystem. Figure 7 shows a set of generalized coordinates of the RAS beam, forming vector $\mathbf{q}_{ra}= \mathrm{col}(q_{1,ra}\ q_{2,ra}\ \ldots\ q_{N,ra})$, where $N= 2n_a{+}1$.

Assembling of the finite elements results in the elastic energy and the kinetic energy of the RAS subsystem as

$$E_{s,ra} = \frac{1}{2}\mathbf{q}_{ra}^T\mathbf{K}_{ra}\mathbf{q}_{ra}, \qquad E_{k,ra} = \frac{1}{2}\dot{\mathbf{q}}_{ra}^T\mathbf{B}_{ra}\dot{\mathbf{q}}_{ra} \tag{26}$$

where

$$\begin{aligned}[\mathbf{K_{ra}}]_{ij} &:= [\mathbf{K_{ra}}]_{ij} + [\mathbf{K}_e]_{i'j'}\,,\\ [\mathbf{B}_{ra}]_{ij} &:= [\mathbf{B}_{ra}]_{ij} + [\mathbf{B}_e]_{i'j'}\,,\end{aligned} \tag{27}$$

wherein $i = i\,(i')$, $j = j(j')$ are determined by respective incidence matrix $\mathbf{q}_{ra}/\mathbf{q}_e$; $e = 1, 2, \ldots, n_a$; $i', j' = 1', 2', 3', 4'$.

The damping power of the RAS beam and the damping matrix in accordance with the Rayleigh model have the form

$$\Phi_{ra} = \frac{1}{2}\dot{\mathbf{q}}_{ra}^T\mathbf{C}_{ra}\dot{\mathbf{q}}_{ra}, \qquad \mathbf{C}_{ra}{=}\mu_a\mathbf{B}_{ra} + \kappa_a\mathbf{K}_{ra} \tag{28}$$

where μ_a, κ_a are coefficients determined by the Eqs. (21).

Load of the RAS beam are appropriate subsets of interaction forces transmitted through the ballast and interaction forces transmitted through the subsoil (Figs. 3, 9). The forces charging the RAS beam are collected below:

$$\begin{gathered}R_{(j)b}\,;\ (j) = (1)\,(2)\,, \ldots, (n_a{+}1)\,;\\ (j) = j + n_a + n_b + n{+}3; \qquad j{=}\ 1, 2, \ldots, n_a{+}1,\\ R_{(j)g}\,;\ (j) = (1)\,(2)\,, \ldots, (n_a)\,;\\ (j) = j + n_a + n_b{+}1; \qquad j{=}\ 1, 2, \ldots, n_a.\end{gathered}$$

The virtual work of these forces on vertical displacements of the RAS beam is

$$L_{ra} = \mathbf{q}_{ra}^T\mathbf{F}_{ra}, \tag{29}$$

where

$$\begin{aligned}\mathbf{F}_{ra}{=}\ \mathrm{col}(0\ R_{(2)b}{-}R_{(1)g}\ 0\ R_{(3)b}\\ -R_{(2)g}\ 0\ \ldots\ 0\ R_{(n_a+1)b}{-}R_{(n_a)g}).\end{aligned} \tag{30}$$

After inserting forms (26), $(28)_1$, (29) for the Lagrange equations of the second kind, i.e.

$$\begin{aligned}\frac{d}{dt}\mathrm{grad}\,E_{k,ra}\,(\dot{\mathbf{q}}_{ra}) + \mathrm{grad}\,\Phi_{ra}\,(\dot{\mathbf{q}}_{ra})\\ + \mathrm{grad}\,E_{s,ra}\,(\mathbf{q}_{ra}) = \mathrm{grad}\,L_{ra}(\mathbf{q}_{ra})\end{aligned} \tag{31}$$

one obtains a matrix equation of motion of the RAS subsystem partly in implicit form, i.e.

$$\mathbf{B}_{ra}\ddot{\mathbf{q}}_{ra} + \mathbf{C}_{ra}\dot{\mathbf{q}}_{ra} + \mathbf{K}_{ra}\mathbf{q}_{ra} = \mathbf{F}_{ra}. \tag{32}$$

Left ballast – bed (LB). A discrete model of the ballast-bed in the LB zone has length 2D. This is a collection of concentrated masses M_b vibrating vertically and loaded by relevant subsets of interaction forces, carried by the ballast and the subsoil, respectively (Fig. 3, 6, 9). The LB subsystem is described by parameters $2D$, d and M_b – ballast mass per one sleeper, $n_b + 1$ – number of concentrated masses.

Figure 6 shows a set of generalized coordinates of the LB subsystem, creating vector $\mathbf{q}_{lb}= \mathrm{col}(q_{1,lb}\ q_{2,lb} \dots\ q_{N,lb})$, where $N = n_b + 1$. The kinetic energy and the mass matrix are

$$E_{k.lb} = \frac{1}{2}\dot{\mathbf{q}}_{lb}^T \mathbf{B}_{lb}\dot{\mathbf{q}}_{lb}, \qquad \mathbf{B}_{lb}= \{\mathbf{M}_b\} = \mathrm{diag}\,(M_b\ M_b \dots\ M_b). \tag{33}$$

The LB subsystem is charged by the R_{jb}, R_{jg}, $j = 1, 2, \dots, N$ forces. The virtual work of these forces on respective vertical displacements and the generalized load vector are defined as

$$L_{lb} = \mathbf{q}_{lb}^T \mathbf{F}_{lb}, \qquad \mathbf{F}_{lb}= \mathrm{col}(R_{1b}-R_{1g}\ R_{2b}-R_{2g}\ \dots\ R_{Nb}-R_{Ng}). \tag{34}$$

After inserting forms $(33)_1$, $(34)_1$ for the Lagrange equations of the first kind, i.e.

$$\frac{d}{dt}\mathrm{grad}\, E_{k,lb}\,(\dot{\mathbf{q}}_{lb}) = \mathrm{grad}\, L_{lb}(\mathbf{q}_{lb}) \tag{35}$$

one obtains a matrix equation of motion of the LB subsystem partly in implicit form, i.e.

$$\{\mathbf{M}_b\}\,\ddot{\mathbf{q}}_{lb} = \mathbf{F}_{lb}. \tag{36}$$

Right ballast – bed (RB). Physical and mathematical modelling of ballast-bed in the RB zone is analogous to modelling of the LB ballast-bed. Ballast-bed RB in the right zone is modelled as a set of concentrated masses M_b vibrating vertically and loaded by relevant subsets of interaction forces, carried by the ballast and the subsoil (Figs. 7, 10). The RB subsystem is described by parameters analogous to those for the LB subsystem.

Figure 7 shows a set of generalized coordinates corresponding to the RB subsystem, creating vector

$$\mathbf{q}_{rb}= \mathrm{col}(q_{1,rb}\ q_{2,rb} \dots\ q_{N,rb}),$$

where $N = n_b + 1$. The kinetic energy and the mass matrix equal

$$E_{k.rb} = \frac{1}{2}\dot{\mathbf{q}}_{rb}^T \mathbf{B}_{rb}\dot{\mathbf{q}}_{rb}, \qquad \mathbf{B}_{rb}= \{\mathbf{M}_b\} = \mathrm{diag}\,(M_b\ M_b \dots\ M_b). \tag{37}$$

The RB subsystem is loaded by the following forces

$$R_{(j)b}\,;\ (j) = (1)\,(2)\,, \dots, (N)\,;$$

$$(j) = j + 2n_a + n_b + n{+}4;\ j{=}\ 1, 2, \dots, N,$$

$$R_{(j)g}\,;\ (j) = (1)\,(2)\,, \dots, (N)\,;$$

$$(j) = j + 2n_a + n_b{+}1;\ j{=}\ 1, 2, \dots, N.$$

The virtual work of these forces on vertical displacements of masses M_b and the generalized load vector are defined by the formulae

$$L_{rb} = \mathbf{q}_{rb}^T \mathbf{F}_{rb}, \qquad \mathbf{F}_{rb}= \mathrm{col}(R_{(1)b}-R_{(1)g}\ R_{(2)b}-R_{(2)g}\ \dots\ R_{(N)b}-R_{(N)g}). \tag{38}$$

After inserting forms $(37)_1$, $(38)_1$ for the Lagrange equations of the first kind, i.e.

$$\frac{d}{dt}\mathrm{grad}\, E_{k,rb}\,(\dot{\mathbf{q}}_{rb}) = \mathrm{grad}\, L_{rb}(\mathbf{q}_{rb}) \tag{39}$$

one obtains a matrix equation of motion of the RB subsystem partly in implicit form, i.e.

$$\{\mathbf{M}_b\}\,\ddot{\mathbf{q}}_{rb} = \mathbf{F}_{rb}. \tag{40}$$

Sleepers (SL). Sleepers are modelled as concentrated masses vibrating vertically and loaded with a set of interactions forces carried by the rail fasteners and the ballast (Figs. 3, 6, 7, 9, 10). Vibrations of the SL subsystem are described by a matrix equation of motion, partly in implicit form, as a direct result of the d'Alembert principle, i.e.

$$\{\mathbf{M}_s\}\,\ddot{\mathbf{q}}_s = \mathbf{F}_s, \tag{41}$$

where

$$\begin{aligned} \{\mathbf{M}_s\} &= \mathrm{diag}\,(M_s\ M_s \dots\ M_s), \\ \mathbf{q}_s &= \mathrm{col}\,(q_{1s}\ q_{2s}\ \dots\ q_{n_t s}), \\ \mathbf{F}_s &= \mathbf{R}_f - \mathbf{R}_b\,, \\ \mathbf{R}_f &= \mathrm{col}\,(R_{1f}\ R_{2f}\ \dots\ R_{n_t f})\,, \\ \mathbf{R}_b &= \mathrm{col}\,(R_{1b}\ R_{2b}\ \dots\ R_{n_t b}), \end{aligned} \tag{42}$$

wherein

$$n_t = 2n_a{+}2n_b + n{+}5,$$

$\mathbf{R}_f$ – interaction force vector transmitted via fasteners, $\mathbf{R}_b$ – interaction force vector carried by ballast $\mathbf{q}_s$ – generalized displacement vector describing SL subsystem.

Operating rails (OR). Operating rails are reflected by an Euler prismatic beam which is fixed to the ends (Fig. 3). The beam is supported viscoelastically via a set of discrete constraints modelling rail fasteners at d intervals. The beam is loaded by moving rail vehicles. Natural damping of vibrations of operating rails is described by the Rayleigh model. The OR subsystem is specified by parameter d and (Figs. 1, 3, 6, 7) $L_t = 4D + L_o$ – length of rails, m_r – mass of pair of rails per unit length, $E_r I_r$ – flexural stiffness of pair of rails, γ_r – quasi-constant damping ratio in frequency range $[f_l f_u]$, μ_r, κ_r – damping coefficients in Rayleigh model, $N_t = 2n_a{+}2n_b + n{+}6$ – number of finite elements of length d.

The finite element nodes correspond to positions of sleepers used in steps d. The bent Euler beam finite element with 4DOF is used (Fig. 5). Deflection of an e-element is described by Eqs. (1), (2). The elastic energy and the kinetic energy of an e-element are described by Eqs. (3)–(5), in which should be substituted

$$EI_e = E_r I_r, \qquad m_e = m_r. \tag{43}$$

Figures 6, 7, show a set of generalized coordinates of the OR beam, forming vector $\mathbf{q}_r= \mathrm{col}\,(q_{1r}\ q_{2r}\ \dots\ q_{Nr})$, wherein $N = 2\,(N_t - 1)$.

Assembling of finite elements forming the OR beam leads to the elastic energy and the kinetic energy of the subsystem described by the formulas

$$E_{sr} = \frac{1}{2}\mathbf{q}_r^T \mathbf{K}_r \mathbf{q}_r, \qquad E_{kr} = \frac{1}{2}\dot{\mathbf{q}}_r^T \mathbf{B}_r \dot{\mathbf{q}}_r \quad . \tag{44}$$

The stiffness matrix $\mathbf{K}_r$ and the mass matrix $\mathbf{B}_r$ have band symmetrical structure with band width of 4. The assembling follows the formulas:

$$\begin{aligned} [\mathbf{K}_r]_{ij} &:= [\mathbf{K}_r]_{ij} + [\mathbf{K}_e]_{i'j'}, \\ [\mathbf{B}_r]_{ij} &:= [\mathbf{B}_r]_{ij} + [\mathbf{B}_e]_{i'j'} \end{aligned} \tag{45}$$

while $i = i\,(i')$, $j = j\,(j')$ are defined by respective incidence matrix $\mathbf{q}_r/\mathbf{q}_e$; $e = 1, 2, \ldots, N_t$; $i'j' = 1', 2', 3', 4'$.

The damping power of the OR beam and the damping matrix in accordance with the Rayleigh model take the form

$$\Phi_r = \frac{1}{2}\dot{\mathbf{q}}_r^T \mathbf{C}_r \dot{\mathbf{q}}_r, \qquad \mathbf{C}_r = \mu_r \mathbf{B}_r + \kappa_r \mathbf{K}_r \tag{46}$$

where, vide Eq. (11)

$$\mu_r = 4\pi\gamma_r \frac{f_l f_u}{f_l + f_u}, \qquad \kappa_r = \frac{\gamma_r}{\pi}\frac{1}{f_l + f_u}. \tag{47}$$

Load of the OR subsystem constitute interaction forces carried by the rail fasteners, i.e. $\mathbf{R}_f = \mathrm{col}\,(R_{1f}\ R_{2f}\ \ldots\ R_{n_t f})$ and moving pressure forces of the wheel sets, i.e. $\mathbf{R}_{wi} = \mathrm{col}\,(R_{1i}\ R_{2i}\ R_{3i}\ R_{4i})$, $i = 1, 2, \ldots, N_v$. The virtual work of forces R_{ki}, $k = 1, 2, 3, 4$ is (Fig. 11)

$$\begin{aligned} L_{ki} &= R_{ki}\,(w_{ki} + r_{ki}) = w_{ki}R_{ki} + r_{ki}R_{ki} \\ &= w_e\,(\overline{x}_{ki}, t)\,R_{ki} + r_{ki}R_{ki} \\ &= \mathbf{q}_e^T\,(t)\,\mathbf{s}\,(\overline{x}_{ki})\,R_{ki} + r_{ki}R_{ki}, \end{aligned} \tag{48}$$

where

$$e = \begin{cases} 0 & u_{ki} \leq 0, \\ [u_{ki}/d] + 1, & 0 < u_{ki} < 4D + L_o, \\ 0, & u_{ki} \geq 4D + L_o, \end{cases} \tag{49}$$

$$\overline{x}_{ki} = u_{ki} - d\,(e-1)$$

and

$$r_{ki} = r\,(u_{ki}) \tag{50}$$

with the following quantities for k-th wheel set of i-th vehicle at time t: u_{ki} – abscissa x; $w_{ki} = w_e\,(\overline{x}_{ki}, t)$ – deflection of e-th finite element; r_{ki} – vertical irregularity of the track.

A random sample of track irregularities is generally illustrated in Fig. 2. By using Figs. 6, 7, 9–11 and Eqs. (48)–(50), one can calculate the virtual work of the loads $\mathbf{R}_f, \mathbf{R}_{wi}, i = 1, 2, \ldots, N_v$ on vertical displacements of the operating rails, which accounts to

$$L_r = \mathbf{q}_r^T \mathbf{F}_{fr} + \sum_{i=1}^{N_v}\sum_{k=1}^{4} L_{ki} = \mathbf{q}_r^T \mathbf{F}_r, \tag{51}$$

where

$$\begin{aligned} \mathbf{F}_r &= \mathbf{F}_{fr} + \mathbf{F}_{vr}, \\ \mathbf{F}_{fr} &= \mathrm{col}\,(-\mathbf{R}_{1f}\ \ 0\ \ -\mathbf{R}_{2f}\ \ 0\ \ldots\ -\mathbf{R}_{n_t f}\ \ 0), \\ [\mathbf{F}_{vr}]_j &:= [\mathbf{F}_{vr}]_j + \sum_{i=1}^{N_v}\sum_{k=1}^{4} s_{j'}\,(\overline{x}_{ki})\,R_{ki}, \end{aligned} \tag{52}$$

wherein $j = j(ej')$ according to respective incidence matrix $\mathbf{q}_r/\mathbf{q}_e$, $e = e\,(u_{ki})$ according to Eq. $(49)_1$, $j' = 1', 2', 3', 4'$. If $e\,(u_{ki}) = 0$, the respective components in double sum are equal to zero. Before starting substitution operation in Eq. $(52)_3$, one must take $\mathbf{F}_{vr} = \mathbf{0}$.

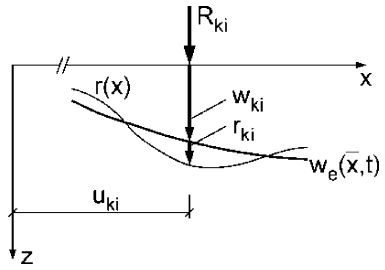

Fig. 11. Pressure force R_{ki} and following vertical displacement

After inserting Eqs. (44), $(46)_1$, (51) for the Lagrange equations of the second kind, i.e.

$$\begin{aligned} &\frac{d}{dt}\mathrm{grad}\,E_{kr}\,(\dot{\mathbf{q}}_r) + \mathrm{grad}\,\Phi_r\,(\dot{\mathbf{q}}_r) \\ &+ \mathrm{grad}\,E_{sr}\,(\mathbf{q}_r) = \mathrm{grad}\,L_r(\mathbf{q}_r) \end{aligned} \tag{53}$$

one obtains a matrix equation of motion of the OR subsystem partly in implicit form, i.e.

$$\mathbf{B}_r \ddot{\mathbf{q}}_r + \mathbf{C}_r \dot{\mathbf{q}}_r + \mathbf{K}_r \mathbf{q}_r = \mathbf{F}_r. \tag{54}$$

Side rails (SR). Modelling of side rails is analogous to modelling of operating rails. The side rails include the bridge span and the approach zones (Fig. 3). The side rails model is an Euler beam supported viscoelastically. Rail fasteners are vertical, discrete, physically nonlinear constraints, at intervals d. Damping of the side rails is described by the Rayleigh model. The SR subsystem is defined by parameters m_r, E_r, I_r, γ_r, μ_r, κ_r, d and (Figs. 3, 6, 7, 9, 10): $L_o = L + 2L_a + 2d$ – length, $N_s = n + 2n_a + 2$ – number of beam finite elements of length d.

Equations (1)–(5), (43) remain valid. Figures 6, 7 show a set of generalized coordinates describing the SR beam, forming vector $\mathbf{q}_{sr} = \mathrm{col}\,(q_{1,sr}\ q_{2,sr}\ \ldots\ q_{N,sr})$, wherein $N = 2N_s + 2$.

Assembling of the finite elements forming the SR beam leads to the elastic energy and the kinetic energy of the SR subsystem described by formulas

$$E_{s,sr} = \frac{1}{2}\mathbf{q}_{sr}^T \mathbf{K}_{sr} \mathbf{q}_{sr}, \qquad E_{k,sr} = \frac{1}{2}\dot{\mathbf{q}}_{sr}^T \mathbf{B}_{sr} \dot{\mathbf{q}}_{sr}. \tag{55}$$

The stiffness matrix $\mathbf{K}_{sr}$ and the mass matrix $\mathbf{B}_{sr}$ have band symmetrical structure with band width of 4. The assembling follows the formulas:

$$\begin{aligned} [\mathbf{K}_{sr}]_{ij} &:= [\mathbf{K}_{sr}]_{ij} + [\mathbf{K}_e]_{i'j'}, \\ [\mathbf{B}_{sr}]_{ij} &:= [\mathbf{B}_{sr}]_{ij} + [\mathbf{B}_e]_{i'j'} \end{aligned} \tag{56}$$

while $i = i\,(i')$, $j = j\,(j')$ are described by respective incidence matrix $\mathbf{q}_{sr}/\mathbf{q}_e$; $e = 1, 2, \ldots, N_s$; $i', j' = 1', 2', 3', 4'$.

The damping power of the SR beam and the damping matrix in accordance with the Rayleigh model are in the form

$$\Phi_{sr} = \frac{1}{2}\dot{\mathbf{q}}_{sr}^T \mathbf{C}_{sr}\dot{\mathbf{q}}_{sr}, \qquad \mathbf{C}_{sr} = \mu_r \mathbf{B}_{sr} + \kappa_r \mathbf{K}_{sr} \tag{57}$$

with coefficients μ_r, κ_r determined by Eqs. (47).

Interaction forces carried by the rail fasteners constitute load of the SR beam, i.e.

$$\mathbf{R}_{sf} = \mathrm{col}\,(R_{1,sf}\ R_{2,sf}\ \ldots\ R_{n_{sf},sf}),$$

where $n_{sf} = N_s + 1$ (Figs. 9, 10). The virtual work of these forces on vertical displacements of the side rails, and the generalized load vector are defined as

$$L_{sr} = \mathbf{q}_{sr}^T \mathbf{F}_{sr},$$
$$\mathbf{F}_{sr} = \mathrm{col}\,(-R_{1,sf}\ 0\ -R_{2,sf}\ 0\ \ldots\ -R_{\mathrm{n_{sf}},sf}\ 0). \tag{58}$$

After inserting forms (55), $(57)_1$, $(58)_1$ for the Lagrange equations of the second kind, i.e.

$$\frac{d}{dt}\mathrm{grad}\, E_{k,sr}\,(\dot{\mathbf{q}}_{sr}) + \mathrm{grad}\,\Phi_{sr}\,(\dot{\mathbf{q}}_{sr}) + \mathrm{grad}\, E_{s,sr}\,(\mathbf{q}_{sr}) = \mathrm{grad}\, L_{sr}(\mathbf{q}_{sr}) \tag{59}$$

one obtains a matrix equation of motion of the SR subsystem partly in implicit form, i.e.:

$$\mathbf{B}_{sr}\ddot{\mathbf{q}}_{sr} + \mathbf{C}_{sr}\dot{\mathbf{q}}_{sr} + \mathbf{K}_{sr}\mathbf{q}_{sr} = \mathbf{F}_{sr}. \tag{60}$$

Railway vehicles (RV$\mathbf{i}$, $\mathbf{i} = 1, 2, \ldots, \mathbf{N_v}$). The enhanced Matsuura model of a four-axle rail-vehicle is defined as follows (Figs. 12, 13):

- Wheel sets are modelled as point masses vibrating vertically, each with 1DOF.
- Bogie frames are modelled as rigid disks, each with 2DOF (vertical translation and in-plane rotation).
- The body is modelled as a rigid disk with 2DOF (vertical translation and in-plane rotation).
- Suspensions of the first and second stage are linear viscoelastic.
- The first-stage suspension pivots are at the same height as the bogie mass centre. The second-stage suspension pivots are at the same height as the body mass centre.
- Masses modelling wheel sets are fitted with one-sided vertical springs of the Hertzian contact stiffness reflecting the wheel set – rails contact.

An RVi rail-vehicle is described by the following parameters: l – total length of rail-vehicle, $2a$ – axial spacing of trucks, $2b$ – axial spacing of wheel sets in each truck, M_c, J_c – mass and central polar moment of inertia of body, M_f, J_f – mass and central polar moment of inertia of bogie frame, M_w – mass of wheel set, k_p, c_p – stiffness and viscous damping coefficient of first-stage suspension, corresponding to one wheel set, k_s, c_s – stiffness and viscous damping coefficient of second-stage suspension, corresponding to one truck, k_H – physically nonlinear Hertz contact stiffness coefficient, corresponding to one wheel set.

An i^{th} rail-vehicle is a discrete system with 10DOF which correspond to generalized coordinate vector $\mathbf{q}_i = \mathrm{col}\,(q_{1i}\ q_{2i}\ \ldots\ q_{10,i})$. At the initial instant, distances of wheel sets from the origin of the xz coordinate system are

$$d_{1i} = (i-1)\,L_v, \qquad d_{2i} = d_{1i} + 2b,$$
$$d_{3i} = d_{1i} + 2a, \qquad d_{4i} = d_{2i} + 2a. \tag{61}$$

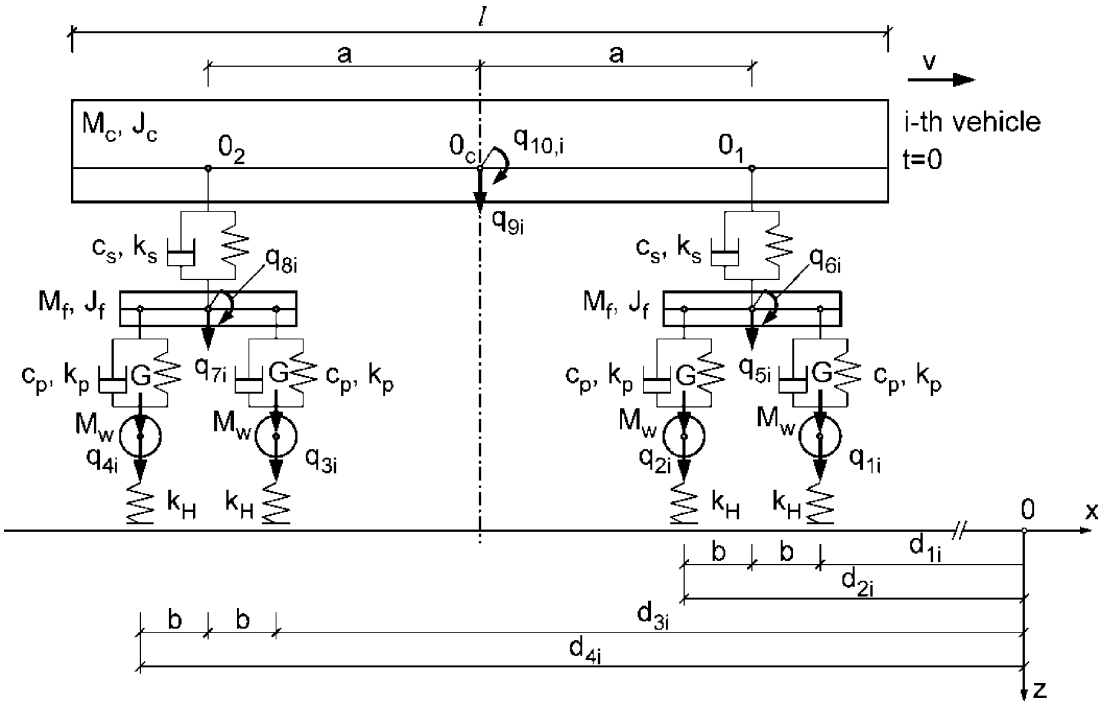

Fig. 12. Enhanced Matsuura model of rail-vehicle and its position at $t = 0$

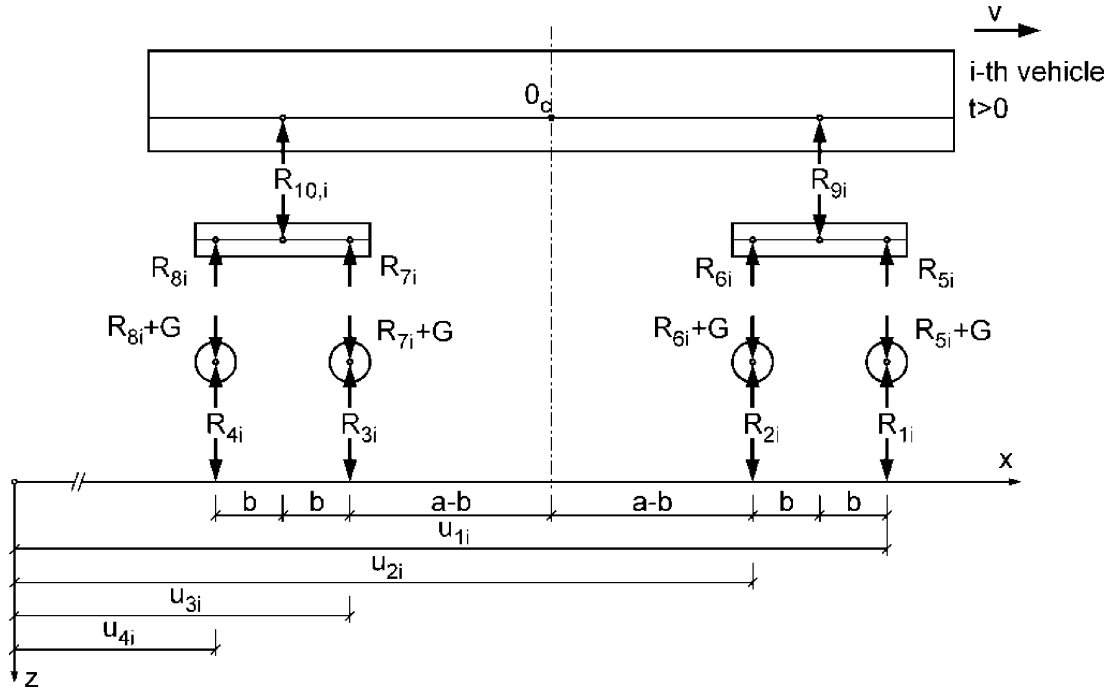

Fig. 13. Interaction forces carried by Hertz contact springs and first- and second-stage suspensions

The kinetic energy of rigid mass elements of the i^{th} vehicle and the mass matrix are

$$E_{ki} = \frac{1}{2}\dot{\mathbf{q}}_i^T \mathbf{B}_i \dot{\mathbf{q}}_i, \tag{62}$$

$$\mathbf{B}_i = \text{diag}\,(M_w\ M_w\ M_w\ M_w\ M_f\ J_f\ M_f\ J_f\ M_c\ J_c)_i\,.$$

Rigid mass elements of an i^{th} vehicle are loaded with vertical interaction forces transmitted by the contact springs and the first- and second-stage suspensions (Fig. 13). These forces create vector $\mathbf{R}_i = \text{col}\,(R_{1i}\ R_{2i}\ \ldots\ R_{10,i})$. The local displacement vector for $\mathbf{R}_i$ forces is

$$\mathbf{u}_i = \text{col}\,(u_{1i}\ u_{2i}\ \ldots\ u_{10,i}) = \mathbf{A}\mathbf{q}_i, \tag{63}$$

where

$$\mathbf{A} = \begin{bmatrix} -1 & 0 & 0 & 0 & 0 & 0 & 0 & 0 & 0 & 0 \\ 0 & -1 & 0 & 0 & 0 & 0 & 0 & 0 & 0 & 0 \\ 0 & 0 & -1 & 0 & 0 & 0 & 0 & 0 & 0 & 0 \\ 0 & 0 & 0 & -1 & 0 & 0 & 0 & 0 & 0 & 0 \\ 1 & 0 & 0 & 0 & -1 & -b & 0 & 0 & 0 & 0 \\ 0 & 1 & 0 & 0 & -1 & b & 0 & 0 & 0 & 0 \\ 0 & 0 & 1 & 0 & 0 & 0 & -1 & -b & 0 & 0 \\ 0 & 0 & 0 & 1 & 0 & 0 & -1 & b & 0 & 0 \\ 0 & 0 & 0 & 0 & 1 & 0 & 0 & 0 & -1 & -a \\ 0 & 0 & 0 & 0 & 0 & 0 & 1 & 0 & -1 & a \end{bmatrix}. \tag{64}$$

The virtual work of $\mathbf{R}_i$ forces on local displacements $\mathbf{u}_i$ as well as of $\mathbf{G}$ forces on vertical displacements of wheel sets and the generalized load vector are described by the formulae

$$L_i = \mathbf{u}_i^T \mathbf{R}_i + \mathbf{q}_i^T \mathbf{G} = \mathbf{q}_i^T \mathbf{A}^T \mathbf{R}_i + \mathbf{q}_i^T \mathbf{G} = \mathbf{q}_i^T \mathbf{F}_i,$$
$$\mathbf{F}_i = \mathbf{A}^T \mathbf{R}_i + \mathbf{G}, \tag{65}$$

where

$$\mathbf{G} = \text{col}\,(G\ G\ G\ G\ 0\ 0\ 0\ 0\ 0\ 0)\,. \tag{66}$$

After inserting forms $(62)_1$, $(65)_1$ for the Lagrange equations of the first kind, i.e.

$$\frac{d}{dt}\text{grad}\,E_{ki}\,(\dot{\mathbf{q}}_i) = \text{grad}\,L_i(\mathbf{q}_i) \tag{67}$$

one obtains a matrix equation of motion of the RVi subsystem partly in implicit form, i.e.

$$\mathbf{B}_i \ddot{\mathbf{q}}_i = \mathbf{F}_i, \qquad i = 1, 2, \ldots, N_v. \tag{68}$$

2.4. Wheel – rail contact stiffness and random vertical track irregularities. Advanced modelling of the wheel – rail contact stiffness according to the Hertz theory is presented by Lei and Noda [2]. Wheel – rail contact is considered as two elastic contact cylinders perpendicular to each other. The relative vertical displacement (shortening is positive) between the wheel and the rail is calculated from the conventional Hertz formula

$$u_H = d_H R_1^{2/3}, \tag{69}$$

where u_H – vertical shortening, $d_H = 1/k_H$ – contact compliance, k_H – contact stiffness, $R_1 = 0.5R$ – half of the interaction force per wheel set.

The inverse formula to equation (69) has the form

$$R_1 = (k_H u_H)^{3/2}\,. \tag{70}$$

The wheel – rail contact compliance equals:

- for new conical wheel tread:

$$d_H = 4.57 r_w^{-0.149} \times 10^{-8} \quad \left[\frac{\text{m}}{\text{N}^{2/3}}\right], \tag{71}$$

- for the wheel of worn tread:

$$d_H = 3.86 r_w^{-0.115} \times 10^{-8} \quad \left[\frac{\mathrm{m}}{\mathrm{N}^{2/3}}\right], \tag{72}$$

where r_w [m] – nominal wheel radius. For an ICE-3 train wheel radius $r_w = 0.46$ m and:

- for new conical wheel tread: $k_H = 0.195 \times 10^8 \left[\frac{\mathrm{N}^{2/3}}{\mathrm{m}}\right]$
- for the wheel of worn tread: $k_H = 0.237 \times 10^8 \left[\frac{\mathrm{N}^{2/3}}{\mathrm{m}}\right]$.

In [16], the average value is used, i.e. $k_H = 0.216 \times 10^8 \left[\frac{\mathrm{N}^{2/3}}{\mathrm{m}}\right]$.

In reference to modelling of random track irregularity samples, only the vertical profile (elevation irregularity), i.e. the mean vertical elevation of two rails, is taken into consideration. Short wavelength corrugation irregularities in rail and design geometry irregularities in track formation are neglected. A stationary and ergodic Gaussian process in space is characterised by one-sided PSD function $S_{rr}(\Omega)$, with $\Omega = 2\pi/L_r$ [rad/m] as a spatial frequency, and L_r as wavelength. The most common definition of $S_{rr}(\Omega)$ is presented by Fryba [18] and was elaborated by Federal Railroad Administration (FRA USA), in the form

$$S_{rr}(\Omega) = kA \frac{\Omega_c^2}{\left(\Omega^2 + \Omega_c^2\right)\Omega^2} \quad \left[\frac{\mathrm{mm^2 m}}{\mathrm{rad}}\right], \tag{73}$$

where $k = 0.25$, $\Omega_c = 0.8245$ [rad/m]. Coefficient A [mm^{2}rad/m] is specified for line grades 1 – 6. Only better railway lines of grades 4 ($A = 53.76$), 5 ($A = 20.95$) and 6 ($A = 3.39$) are considered in [16].

Random samples of track irregularity vertical profile are generated with the Monte-Carlo method which results in the following formula [18]

$$r(x) = 2\sum_{i=1}^{N_r} \sqrt{S_{rr}(\Omega_i)\,\Delta\Omega} \cos(\Omega_i x + \phi_i) \quad [\mathrm{mm}], \tag{74}$$

where $\Omega_i = \Omega_{\min} + (i - 0.5)\Delta\Omega$ – discrete frequency, ϕ_i – random phase angle uniformly distributed over $[0,\, 2\pi]$ [rad] interval and independent for $i = 1, 2, \ldots, N_r$, $\Delta\Omega = \dfrac{1}{N_r}(\Omega_{\max} - \Omega_{\min})$ – frequency increment, N_r – total number of frequency increments in $[\Omega_{\min}, \Omega_{\max}]$ interval, $\Omega_{\min} = \dfrac{2\pi}{L_{r,\max}}$ $\Omega_{\max} = \dfrac{2\pi}{L_{r,\min}}$ – lower and upper limits of spatial frequency, $L_{r,\min}, L_{r,\max}$ – lower and upper limits of wavelength.

2.5. Interaction forces. A non-linear elastic characteristic of rail fastenings is illustrated in Fig. 14. In simulations chart b) should be taken, i.e. taking into account the compression of static weight of the rails. Interactive force $\mathbf{R}_f$ is positive when the vertical constraints are shortened by the value of u and equals

$$R_f(u,\dot{u}) = \begin{cases} k_{f1}u + c_f\dot{u}, \\ \qquad -u_{fo} \le u \le u_f - u_{fo}, \\ k_{f1}(u_f - u_{fo}) + k_{f2}[u - (u_f - u_{fo})] + c_f\dot{u}, \\ \qquad u > u_f - u_{fo}, \\ k_{f1}(-u_{fo}) + k_{f3}(u + u_{fo}) + c_f\dot{u}, \\ \qquad u < -u_{fo}, \end{cases} \tag{75}$$

where

$$u_{fo} = \frac{M_r g}{k_{f1}}. \tag{76}$$

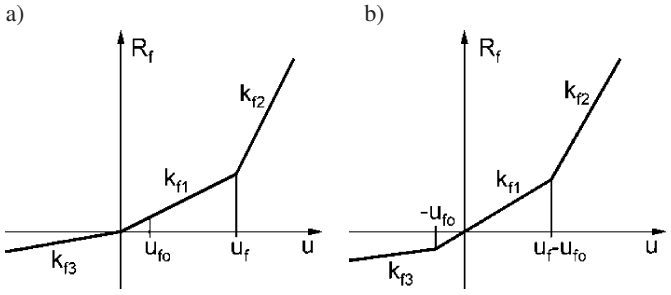

Fig. 14. Elastic characteristic of rail fastenings: a) before taking into account static compression induced by rails weight, b) after taking into account static compression induced by rails weight

A non-linear elastic characteristic of the ballast-bed layer is illustrated in Fig. 15. In the simulations, chart b) should be taken, i.e. taking into account the compression resulting from the static weight of rails and sleepers. The interactive force R_b is positive when the vertical constraints are shortened by value of u and equals

$$R_b(u,\dot{u}) = \begin{cases} k_{b1}u + c_b\dot{u}, & u \ge -u_{bo}, \\ k_{b1}(-u_{bo}) + c_b\dot{u}, & u < -u_{bo}, \end{cases} \tag{77}$$

where

$$u_{bo} = \begin{cases} \frac{(2M_r + M_s)g}{k_{b1}}, & x \in [2D;\, 2D + L_o], \\ \frac{(M_r + M_s)g}{k_{b1}}, & x \in [0;\, 4D + L_o] \setminus [2D;\, 2D + L_o]. \end{cases} \tag{78}$$

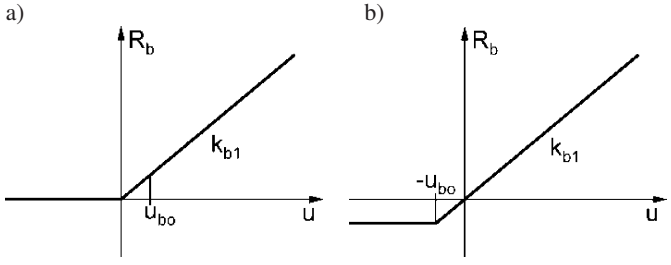

Fig. 15. Elastic characteristic of ballast layer: a) before taking into account static compression induced by weight of rails, b) after taking into account static compression induced by weight of rails

Interaction forces carried by rail fasteners of operating rails create the vector

$$\mathbf{R}_f = \mathrm{col}\,(R_{1f}\ R_{2f} \ldots R_{n_t f}), \qquad \dim \mathbf{R}_f = n_t = 2n_b + 2n_a + n + 5. \tag{79}$$

The R_{jf} forces are defined by the Eq. (75), wherein

$$R_{jf} = R_f\left(u_j, \dot{u}_j\right), \qquad u_j = q_{r,2j-1} - q_{sj}, \qquad j = 1, 2, \ldots, n_t. \tag{80}$$

Interaction forces carried by the ballast-bed create the vector

$$\mathbf{R}_b = \operatorname{col}\left(R_{1b}\ R_{2b} \ldots R_{n_t b}\right), \qquad \dim \mathbf{R}_b = n_t = 2n_b + 2n_a + n + 5. \tag{81}$$

The R_{jb} forces are defined by the Eq. (77), wherein

$$R_{jb} = R_b\left(u_j, \dot{u}_j\right)$$

$$u_j = \begin{cases} q_{sj} - q_{lb,j}, & j = 1, 2, \ldots, n_b + 1, \\ q_{sj} - q_{la,2i-1}, & i = 1, 2, \ldots, n_a,\ j = n_b + 1 + i, \\ q_{sj}, & j = n_b + n_a + 2, \quad n_b + n_a + 3, \\ & \quad n_b + n_a + n + 3, \quad n_b + n_a + n + 4, \\ q_{sj} - q_{2i}, & i = 1, 2, \ldots, n-1, \\ & \quad j = n_b + n_a + 3 + i, \\ q_{sj} - q_{ra,2i}, & i = 1, 2, \ldots, n_a, \\ & \quad j = n_b + n_a + n + 4 + i, \\ q_{sj} - q_{rb,i}, & i = 1, 2, \ldots, n_b + 1, \\ & \quad j = n_b + 2n_a + n + 4 + i. \end{cases} \tag{82}$$

Interaction forces carried by the subgrade create the vector

$$\mathbf{R}_g = \operatorname{col}\left(R_{1g}\ R_{2g} \ldots R_{n_g g}\right), \qquad \dim \mathbf{R}_g = n_g = 2n_b + 2n_a + 2. \tag{83}$$

The R_{jg} forces are

$$R_{jg} = R_g\left(u_j, \dot{u}_j\right), \qquad R_g\left(u, \dot{u}\right) = k_g u + c_g \dot{u},$$

$$u_j = \begin{cases} q_{lb,j}, & j = 1, 2, \ldots, n_b + 1, \\ q_{la,2i-1}, & i = 1, 2, \ldots, n_a, \quad j = n_b + 1 + i, \\ q_{ra,2i}, & i = 1, 2, \ldots, n_a, \quad j = n_b + n_a + 1 + i, \\ q_{rb,i}, & j = n_b + 2n_a + 1 + i, \quad i = 1, 2, \ldots, n_b + 1. \end{cases} \tag{84}$$

Interaction forces carried by rail fasteners of the side rails create the vector

$$\mathbf{R}_{sf} = \operatorname{col}\left(R_{1,sf}\ R_{2,sf} \ldots R_{n_{sf} sf}\right), \qquad \dim \mathbf{R}_{sf} = n_{sf} = 2n_a + n + 3. \tag{85}$$

The $R_{j,sf}$ forces are defined by the Eq. (75), wherein

$$R_{j,sf} = R_f\left(u_j, \dot{u}_j\right), \qquad u_j = q_{sr,2j-1} - q_{s,n_b+1+j}, \qquad j = 1, 2, \ldots, n_{sf}. \tag{86}$$

Interaction forces charged to the i-th rail-vehicle form the vector

$$\mathbf{R}_i = \operatorname{col}\left(R_{1i}\ R_{2i} \ldots R_{10,i}\right) = \operatorname{col}\left(\mathbf{R}_{wi}\ \mathbf{R}_{si}\right), \tag{87}$$

where $\mathbf{R}_{wi} = \operatorname{col}\left(R_{1i}\ R_{2i}\ R_{3i}\ R_{4i}\right)$ – interaction forces carried by Hertzian contact springs, $\mathbf{R}_{si} = \operatorname{col}\left(R_{5i}\ R_{6i}\ \ldots\ R_{10,i}\right)$ – interaction forces carried by first- and second-stage suspensions.

The $\mathbf{q}_i$ coordinates are measured from the static equilibrium of the i-th rail-vehicle on a rigid straight horizontal track. Contact springs are shortened under the influence of static pressures on the vehicle axles. In the case of an ICE-3 train, all static pressures are equal to $G = 16000\,\mathrm{kg} \times 9.81 \frac{\mathrm{m}}{\mathrm{s}^2} = 156.96$ kN. Thus, static shortening of the contact springs is (*vide* Eq. (69))

$$u_{Ho} = \left(0.5G\right)^{2/3} \Big/ k_H = \left(0.5 \times 156960\right)^{2/3} \Big/ \left(0.216 \times 10^8\right) = 84.86 \times 10^{-6}\,\mathrm{m}. \tag{88}$$

A force transmitted by the contact spring, taking into account the static shortening, is a generalization of Eq. (70). i.e.

$$R\left(u_H\right) = \begin{cases} 2\left[k_H\left(u_H + u_{Ho}\right)\right]^{3/2}, & u_H > -u_{Ho}, \\ 0, & u_H \le u_{Ho}. \end{cases} \tag{89}$$

Elements of the $\mathbf{R}_{wi}$ vector are

$$R_{ki} = R\left(u_{H,ki}\right), \qquad k = 1, 2, 3, 4, \tag{90}$$

where

$$u_{H,ki} = q_{ki} - \left(w_{ki} + r_{ki}\right), \qquad w_{ki} = w_e\left(\overline{x}_{ki}\right), \qquad r_{ki} = r\left(u_{ki}\right), \qquad u_{ki} = vt - d_{ki}. \tag{91}$$

Number e and abscissa $\overline{x}_{ki}$ are defined by the Eqs. (49).

Suspensions of a rail-vehicle are vertical linear viscoelastic constraints. The dynamic interaction force vector carried by these constraints is described in the form

$$\mathbf{R}_{si} = \{\mathbf{k}\}_i \mathbf{u}_i + \{\mathbf{c}\}_i \dot{\mathbf{u}}_i, \tag{92}$$

where

$$\{\mathbf{k}\}_i = \operatorname{diag}\left(k_p\ k_p\ k_p\ k_p\ k_s\ k_s\right)_i, \qquad \{\mathbf{c}\}_i = \operatorname{diag}\left(c_p\ c_p\ c_p\ c_p\ c_s\ c_s\right)_i, \qquad \mathbf{u}_i = \mathbf{A}_s \mathbf{q}_i, \quad \dot{\mathbf{u}}_i = \mathbf{A}_s \dot{\mathbf{q}}_i. \tag{93}$$

Matrix $\mathbf{A}_s$ transforming generalized coordinates $\mathbf{q}_i$ to shortening of the constraints, is the appropriate submatrix of the matrix $\mathbf{A}$ (Eq. (64)) with sign –, i.e

$$\mathbf{A}_s = \begin{bmatrix} -1 & 0 & 0 & 0 & 1 & b & 0 & 0 & 0 & 0 \\ 0 & -1 & 0 & 0 & 1 & -b & 0 & 0 & 0 & 0 \\ 0 & 0 & -1 & 0 & 0 & 0 & 1 & b & 0 & 0 \\ 0 & 0 & 0 & -1 & 0 & 0 & 1 & -b & 0 & 0 \\ 0 & 0 & 0 & 0 & -1 & 0 & 0 & 0 & 1 & a \\ 0 & 0 & 0 & 0 & 0 & 0 & -1 & 0 & 1 & -a \end{bmatrix}. \tag{94}$$

Weights of the sprung masses are imported to wheel sets, hence the initial conditions of the sprung masses are equal zero, i.e.

$$\mathbf{q}_i\left(0\right) = \mathbf{0}, \qquad \dot{\mathbf{q}}_i\left(0\right) = \mathbf{0}, \qquad \ddot{\mathbf{q}}_i\left(0\right) = \mathbf{0}, \qquad i = 1, 2 \ldots, N_v. \tag{95}$$

2.6. Numerical integration of equations of motion. As proved in previous points, transient vibrations of the BTT system are governed by $8 + N_v$ matrix equations of motion, where N_v is number of rail-vehicles. These equations are partly in implicit form. The coupling is hidden in the generalized load vectors expressed by the interaction forces $\mathbf{R}_f$, $\mathbf{R}_{sf}$, $\mathbf{R}_b$, $\mathbf{R}_g$, $\mathbf{R}_i$, $i = 1, 2, \ldots, N_v$. Matrix equations of motion of the subsystems belong to the class of linear ordinary differential equations with constant coefficients, i.e.

$$\mathbf{B}\ddot{\mathbf{q}}(t) + \mathbf{C}\dot{\mathbf{q}}(t) + \mathbf{K}\mathbf{q}(t) = \mathbf{F}\left(\mathbf{R}\left(t\right),t\right), \tag{96}$$

where $\mathbf{B}$, $\mathbf{C}$, $\mathbf{K}$ – mass, damping and stiffness matrices for an inertial subsystem, $\mathbf{F}\left(\mathbf{R}\left(t\right),t\right)$ – generalized load vector, related to a subsystem, generally dependent on interaction forces vector $\mathbf{R}(t)$ and time variable t.

At the initial instant, the train has a constant horizontal operating velocity v and it is on the left straight rigid track. The BTT system is in equilibrium and is described so that each subsystem corresponds to zero initial conditions, i.e.

$$\mathbf{q}\left(0\right) = \mathbf{0}, \qquad \dot{\mathbf{q}}\left(0\right) = \mathbf{0}. \tag{97}$$

In addition, $\mathbf{F}\left(\mathbf{R}\left(0\right),0\right) = \mathbf{0}$, and hence from Eq. (96) at the initial instant one obtains

$$\ddot{\mathbf{q}}\left(0\right) = \mathbf{0}. \tag{98}$$

To date, numerous one-step and multi-step methods for numerical integration of equations of motion of discrete systems have been developed. One-step methods are natural for these equations due to initial conditions. One-step methods are divided into two groups, i.e. methods without numerical (spurious) damping (e.g. a set of Newmark's methods with parameter $\gamma_N = 1/2$) and methods with numerical damping (e.g. a set of Newmark's methods with parameter $\gamma_N \neq 1/2$) [19]. Methods without numerical damping are analysed due to the stability limit, the amplitude error and the period error. A finite stability limit causes a rapid growth of numerical integration errors nearby this limit. The amplitude error influences accuracy, however, it does not accumulate itself during the integration process. The period error crucially influences accuracy since it accumulates itself during the integration process.

The implicit matrix equation of motion (96) will be integrated numerically at initial conditions (97, 98) using the Newmark average acceleration method with parameters β_N=1/4, $\gamma_N = 1/2$, developed to the implicit form as presented in [14]. The amplitude error vanishes, while the period error decreases as a time step decreases. The influence of the period error can be freely reduced via assuming a relatively small integration step determined from preliminary numerical tests. Note that in the case of explicit equations this method is unconditionally stable.

Dynamic response of an N-DOF system described by governing Eq. (96) is determined in equidistant time points in the $[0, T]$ interval, i.e.

$$t_{i+1} = (i{+}1)\,h, \qquad i{=}\,0, 1, \ldots, N_c{-}1, \tag{99}$$

where T is time of the dynamic process duration, $h = \Delta t$ is a time step, $N_c = T/h$ is number of integration steps. The following discrete values are introduced

$$\begin{gathered}\mathbf{q}_i{=}\,\mathbf{q}\left(t_i\right), \qquad \dot{\mathbf{q}}_i = \dot{\mathbf{q}}\left(t_i\right), \qquad \ddot{\mathbf{q}}_i = \ddot{\mathbf{q}}\left(t_i\right), \\ \mathbf{R}_i{=}\,\mathbf{R}\left(t_i\right), \qquad \mathbf{F}_i{=}\,\mathbf{F}\left(\mathbf{R}_i,t_i\right).\end{gathered} \tag{100}$$

The Newmark recurrent formulae for $\beta_N = 1/4$, $\gamma_N = 1/2$ have the form [18]

$$\begin{cases}\mathbf{q}_{i+1} = \mathbf{q}_i + h\dot{\mathbf{q}}_i + \dfrac{1}{4}h^2\left(\ddot{\mathbf{q}}_i + \ddot{\mathbf{q}}_{i+1}\right), \\ \dot{\mathbf{q}}_{i+1} = \dot{\mathbf{q}}_i + \dfrac{1}{2}h\left(\ddot{\mathbf{q}}_i + \ddot{\mathbf{q}}_{i+1}\right).\end{cases} \tag{101}$$

Acceleration vector $\ddot{\mathbf{q}}_{i+1}$ is determined from the collocation condition at the end of the i-th time step what results in an algebraic system of linear equations, i.e.

$$\mathbf{U}\ddot{\mathbf{q}}_{i+1} = \mathbf{V}_{i+1} \Longrightarrow \ddot{\mathbf{q}}_{i+1} = \mathbf{U}^{-1}\mathbf{V}_{i+1}, \tag{102}$$

where

$$\begin{gathered}\mathbf{U} = \mathbf{B}{+}\frac{1}{2}h\mathbf{C}{+}\frac{1}{4}h^2\mathbf{K}, \\ \mathbf{V}_{i+1} = \mathbf{F}_{i+1}{-}\mathbf{C}\left(\dot{\mathbf{q}}_i + \frac{1}{2}h\ddot{\mathbf{q}}_i\right) \\ {-}\,\mathbf{K}\left(\mathbf{q}_i + h\dot{\mathbf{q}}_i + \frac{1}{4}h^2\ddot{\mathbf{q}}_i\right).\end{gathered} \tag{103}$$

Matrix $\mathbf{U}$ is reversed only once. Based on Eqs. (97, 98) the extended initial conditions take the form

$$\mathbf{q}_0 = \mathbf{0}, \qquad \dot{\mathbf{q}}_0 = \mathbf{0}, \qquad \ddot{\mathbf{q}}_0 = \mathbf{0}. \tag{104}$$

An algorithm for numerical integration of Eq. (96) is implicit due to interaction vector $\mathbf{R}_{i+1}$ that defines vector $\mathbf{F}_{i+1}$. A linear prediction of vector $\mathbf{R}_{i+1}$ is used, i.e. [14]

$$\mathbf{R}^{\mathrm{p}}_{i+1}{=}\,2\mathbf{R}_i{-}\,\mathbf{R}_{i-1} \tag{105}$$

with $\mathbf{R}_{-1} = \mathbf{R}_0$ due to static equilibrium of the system in the $t \leq 0$ interval. The implicit algorithm for numerical integration of Eq. (96) consists of the following calculation stages:

1. predict $\mathbf{R}_{i+1}$ using Eq. (105),
2. calculate $\ddot{\mathbf{q}}_{i+1}$ using Eqs. (102), (103) with $\mathbf{R}_{i+1} = \mathbf{R}^{\mathrm{p}}_{i+1}$,
3. calculate $\mathbf{q}_{i+1}$, $\dot{\mathbf{q}}_{i+1}$ using Eqs. (101),
4. correct $\mathbf{R}_{i+1}$ calculating the forces by definitions (one obtains $\mathbf{R}^{\mathrm{c}}_{i+1}$),
5. check the iteration end condition

$$\left|R^c_{j,i+1}{-}R^p_{j,i+1}\right| \leq \varepsilon, \qquad j{=}\,1,\,2,\,\ldots,N, \tag{106}$$

where $\varepsilon > 0$ – accuracy parameter determined from preliminary numerical simulations; if relationship (106) is satisfied, go to next time step; if relationship (106) is not satisfied, substitute

$$\mathbf{R}^{\mathrm{p}}_{i+1} := \mathbf{R}^{\mathrm{c}}_{i+1} \tag{107}$$

and go to stage 2.

3. Conclusions

1. The study develops an advanced theory of 1D quasi-exact physical and mathematical modelling of composite bridge / track structure / high-speed train systems (BTT), including viscoelastic suspensions of rail-vehicles equipped with two two-axle bogies, non-linear Hertz contact stiffness and one-sided contact between the wheel sets and the rails, viscoelastic and inertia features of the bridge, the track structure on and beyond the bridge, approach slabs, and random vertical track irregularities. Compared to the state-of-the-art, the physical model developed in this study accurately reproduces dynamic processes in real systems.
2. A method of formulation of equations of motion partly in implicit form has appeared to be effective for BTT systems. Vibrations in the vertical plane of symmetry are described by more than nine matrix equations of motion with constant coefficients. The couplings and non-linearities are hidden in the generalized load vectors. The equations of motion are of high clearance, easy to mechanical and mathematical interpretations. They are integrated using the implicit Newmark average acceleration method with linear extrapolation of the interaction forces.
3. Simulation of deterministic and random vibrations of the exemplary BTT system is presented in [5, 17].

Acknowledgements. The study was supported by the National Centre for Science, Poland, as a part of the project No. N N506 0992 40, realized in the period 2011-2013. This support is gratefully acknowledged.

REFERENCES

[1] A. Wiriyachai, K.H. Chu, and V.K. Gang, "Bridge impact due to wheel and track irregularities", *ASCE J. Engng. Mech. Div.* 108 (4), 648–666, 1982.

[2] X. Lei and N.-A. Noda, "Analyses of dynamic response of vehicle and track coupling system with random irregularity of track vertical profile", *J. Sound Vib.* 258 (1), 147–165, 2002.

[3] F.T.K. Au, J.J. Wang, and Y.K. Cheung, "Impact study of cable stayed railway bridges with random rail irregularities", *Engineering Structures* 24, 529–541 (2002).

[4] M. Majka and M. Hartnett, "Dynamic response of bridges to moving trains: A study on effects of random track irregularities and bridge skewness", *Comput. Struct.* 87, 1233–1253 (2009).

[5] M. Podworna and M. Klasztorny, "Vertical vibrations of composite bridge / track structure / high-speed train system. Part 1: Series-of-types of steel-concrete bridges", *Bull. Pol. Ac.: Tech.* 62 (1), 165–179 (2014).

[6] M. Klasztorny, *Vibrations of Railway Single-track Bridges Induced by Trains Moving at High-speeds,* WPWr Press, Wroclaw, 1987, (in Polish).

[7] M. Klasztorny, *Dynamics of Beam Bridges under High-speed Trains*, WNT Press, Warsaw, 2005, (in Polish).

[8] L. Fryba, "A rough assessment of railway bridges for high speed trains", *Engineering Structures* 23, 548–556 (2001).

[9] Y.S. Cheng, F.T.K. Au, and Y.K. Cheung, "Vibration of railway bridges under a moving train by using bridge-track-vehicle element", *Engineering Structures* 23 (12), 1597–1606 (2001).

[10] F.T.K. Au, J.J. Wang, and Y.K. Cheung, "Impact study of cable-stayed bridge under railway traffic using various models", *J. Sound Vib.* 240 (3), 447–465 (2001).

[11] Q.-L. Zhang, A. Vrouwenvelder, and J. Wardenier, "Numerical simulation of train – bridge interactive dynamics", *Comput. Struct.* 79, 1059–1075 (2001).

[12] M.-K. Song and C.-K. Choi, "Analysis of high-speed vehicle-bridge interactions by a simplified 3-D model", *Structural Engineering and Mechanics* 13 (5), 505–532 (2002).

[13] M. Podworna, "Vertical vibrations of steel beam bridges induced by trains moving at high speeds. Part 1 – theory", *Archives of Civil Engineering* 51 (2), 179–209 (2005).

[14] M. Podworna, "Vertical vibrations of steel beam bridges induced by trains moving at high speeds. Part 2 – numerical analysis", *Archives of Civil Engineering* 51 (2), 211–231 (2005).

[15] F. Lu, J.H. Lin, D. Kennedy, and F.W. Williams, "An algorithm to study non-stationary random vibrations of vehicle – bridge system", *Comput. Struct.* 87, 177–185 (2009).

[16] J. Langer, *Dynamics of Structures,* Wroclaw Univ. Technol. Press, Wroclaw, 1980, (in Polish).

[17] M. Podworna and M. Klasztorny, "Vertical vibrations of composite bridge / track structure / high-speed train system. Part 3: Deterministic and random vibrations of exemplary system", *Bull. Pol. Ac.: Tech.* 62 (2), (2014), (to be published).

[18] L. Fryba, *Dynamics of Railway Bridges*, Academia, Praha, 1996.

[19] N.M. Newmark, "A method of computation for structural dynamics", *ASCE J. Eng. Mech. Div*. 85 (3), 67–94 (1959).